Compounding seasonal variations in outlet glacier dynamics revealed by high-resolution observations

Enze Zhang[1], Ginny Catania[1,2], Ben Smith[3], Denis Felikson[4], Beata Csatho[5], and Daniel T. Trugman[6]

[1]The University of Texas at Austin, Institute of Geophysics, TX, USA
[2]The University of Texas at Austin, Department of Geological Sciences, TX, USA
[3]Polar Science Center, Applied Physics Laboratory, University of Washington, Seattle, WA, USA
[4]Cryospheric Sciences Laboratory, NASA Goddard Space Flight Center, Greenbelt, MD, USA
[5]Department of Geological Sciences, University at Buffalo, Buffalo, NY, USA
[6]Nevada Seismological Laboratory, Nevada Geosciences, University of Nevada, Reno, NV, USA

Key Points:

- Simple model can be used to attribute a portion of seasonal velocity variability caused by terminus position change.
- Seasonal velocity variability is complex and results from multiple compounding processes.
- Seasonal velocities are more sensitive to surface slope changes than uniform changes in elevation.

Corresponding author: Enze Zhang, `zhangenze@link.cuhk.edu.hk`

Abstract

Understanding seasonality in outlet glacier dynamics reveals insight into long-term retreat and acceleration. Leveraging recent high-resolution satellite data, we examine changes in surface elevation, velocity, and terminus position for five glaciers in Central Western Greenland over the past ∼6 years. We employ an approach that examines the stress at the ice-ocean terminus and models the expected response in upstream velocity caused by the observed terminus changes. The model shows that some glaciers' seasonal velocity changes can be largely explained by terminus changes, while others can be compounded by multiple processes. Additionally, we test the sensitivity of the results by including seasonally varying and artificially modified surface topography. We find surface slope changes impact velocity response to terminus changes more than spatially uniform changes in along-flow elevation. Our approach provides a scalable framework to comprehend the compounded nature of glacier seasonal velocity variations across the Greenland Ice Sheet outlet glaciers.

Plain Language Summary

Understanding seasonal changes in glaciers is crucial for studying long-term trends. To capture glacier seasonality in detail, we combine detailed data on glacier speed and terminus movement at sub-weekly to daily intervals, along with seasonal surface topography data. We use a model that reveals how much glacier speed changes in response to terminus variations. For some glaciers, our model shows that seasonal glacier speed change is completely driven by terminus change. For other glaciers, we find that seasonal velocity changes can be influenced by runoff and seasonal changes in the drainage system beneath the glacier, in addition to terminus position change. Additional tests suggest that change in the surface slope of a glacier has a stronger impact on the sensitivity of seasonal speed changes to terminus changes than uniform changes in glacier surface topography; flattening of the glacier surface results in less sensitivity of the surface velocity to terminus changes. Our approach provides a framework that can be applied to the entire Greenland Ice Sheet to reveal the complexity of glacier seasonality.

1 Introduction

The Greenland Ice Sheet (GrIS) is currently the largest land ice contributor to present-day rising sea level (IPCC, 2022) with an acceleration in mass loss over the past few decades primarily attributed to ice discharge through outlet glaciers (Shepherd et al., 2012; Enderlin et al., 2014; van den Broeke et al., 2016). This acceleration underscores the importance of comprehending the intricate mechanisms that govern glacier dynamics. Despite the prevalence of glacier acceleration in Greenland, there exists notable spatio-temporal variability in glacier velocity change at a range of time scales (Moon et al., 2012, 2020), which is likely influenced by local conditions, like topography, and regionally by environmental factors. For example, runoff and ocean thermal forcing can influence velocity by changing basal friction (Ultee et al., 2022), subaqueous melt rates (Holland et al., 2008), and through terminus fluctuations (Howat et al., 2008; King et al., 2020; Wood et al., 2021). Numerical simulations also suggest a non-linear feedback between terminus changing rate and ice discharge (Sergienko, 2022). At the seasonal scale, many of these processes are synchronized, making it difficult to understand the cause and effect behind seasonal glacier acceleration. Despite this, recent advances in the temporal frequency of satellite measurements provide an opportunity to examine the factors that force glacier dynamic change over multiple epochs (Kehrl et al., 2017). Moreover, numerical simulations suggest that glacier seasonal changes can induce systematic bias in mass loss estimates at the multi-decadal time scale (Felikson et al., 2022). Thus, delving into the patterns of glacier seasonality is instrumental in unveiling and simulating the pivotal factors that control glacier dynamics at longer time scales and into the future.

Glaciers across Greenland exhibit discernible seasonal changes in terminus position (Goliber et al., 2022; Zhang et al., 2023) and surface velocity (Moon et al., 2015; Joughin et al., 2008), but the mechanisms behind such changes are varied. Studies have suggested that seasonal glacier retreat due to summertime air temperature increases causes reduced contact with bed and/or fjord walls, which along with increased net force at the calving cliff, leading to glacier acceleration (Howat et al., 2005; Joughin et al., 2012). Others have indicated that glacier acceleration can be due to seasonal changes in basal lubrication related to changes in the subglacial hydrological system (Davison et al., 2020; Stevens et al., 2022; Werder et al., 2013; Andrews et al., 2014), which can cause complex responses from glacier velocities as subglacial conduits grow more efficient (Bartholomew et al., 2010; Andrews et al., 2014; Vijay et al., 2019). Subglacial hydrology can also be influenced by remnant meltwater (Iken & Truffer, 1997) that is stored englacially (Abe & Furuya, 2015) or in basal crevasses (Harper et al., 2010) and through exfiltrated groundwater (Robel et al., 2023), which can leak out of the subglacial system over time, including in winter (Rennermalm et al., 2013).

Previous efforts have classified glacier seasonal velocity variations into types based on the observed timing of velocity change and their correlation to runoff and terminus change (Moon et al., 2014; Vijay et al., 2019, 2021). Three categories have been generally described in this literature; 1) positive correlation of glacier velocity to glacier terminus retreat; 2) positive correlation of glacier velocity to summer runoff, and; 3) glacier velocity that slows in late summer and speeds up in winter. Recently, Solgaard et al. (2022) applied a machine learning approach to analyze velocity time series data across Greenland, revealing similar seasonal patterns as those first identified by Moon et al. (2014). However, most of these studies used data with limited temporal sampling resulting in classifications that are based on identifying a single process that influences velocity. Poinar (2023) applied principal component analysis to decompose the seasonality of glaciers in Sermilik Fjord from an observational perspective. They emphasized the importance of extracting velocity patterns across the entire glacier, not just a single point. Furthermore, they classified four glaciers in Sermilik Fjord by quantifying the prevalence of multiple glacier types at a single glacier. Here, we re-examine glacier seasonality using high-frequency terminus (Zhang et al., 2023), velocity (Gardner et al., 2023), and surface elevation change observations. We interpret these observations with an analytical model of velocity response to terminus position change (Joughin et al., 2012). By comparing model results with observed velocity time series we find that glaciers are more typically influenced by an interplay of multiple processes rather than a single process, and that glacier velocity behavior can transition between different modes seasonally.

2 Study regions

We investigate five glaciers in central-west Greenland (Figure 1): Rink Isbrae (RNK), Sermeq Avannarleq (AVA), Sermeq Kujalleq (KUJ), Kangilernata Sermia (KAN), and Eqip Sermia (EQP) over the time period 2015-2021. This time span is specifically chosen to take advantage of the increased sample frequency available in both velocity and terminus position data due to the launch of Sentinel-1/2 in 2014. These five glaciers are selected because 1) they exhibit regular seasonal changes in both terminus position and velocity (Catania et al., 2018; Fried et al., 2018) with minimal long-term variations over our study period and; 2) they exhibit a range of sub-seasonal behavior in both the terminus and velocity variability. For example, all glaciers advance in winter and retreat in summer and yet their seasonal velocity behavior differs over time and space. EQP and KUJ speed up during summertime terminus retreat while AVA and KAN slow down during summertime terminus retreat (Fried et al., 2018). AVA, KUJ, KAN, and EQP are located close to one another, suggesting that they likely experience the same regional climate forcing. We also examine RNK, which is further north than these four glaciers because it has a deep grounding line, in contrast to the shallower grounding lines of the other four glaciers to the south, and a partially floating terminus that permits large, buoyant flexure-style calving events driving glacier-wide step changes in the terminus position (Medrzycka et al., 2016; Fried et al., 2018). Medrzycka et al. (2016) investigated the calving styles of RNK by using time-Lapse photos and found that the northern part of the RNK terminus undergoes small calving events, while the southern part experiences larger events driven in response to buoyant flexure. The authors suggested that these buoyancy conditions exert primary control on terminus behavior, implying that the northern part of RNK is lightly grounded, while the southern part is floating.

3 Data

We use dense velocity time series data generated using auto-RIFT (Gardner et al., 2018) and provided by the NASA MEaSUREs ITS_LIVE project (Gardner et al., 2023). ITS_LIVE combines velocity products derived from Landsat-8, Sentinel-1, and Sentinel-2 producing a near-daily temporal resolution since 2014. For each glacier, we use multiple flowlines across the glacier from Felikson et al. (2021) to extract velocities at multiple points along each flowline (red and blue points in Figure 1). We then average these velocities across all flowlines at each cross-section to produce mean (across-flow) velocity time series from downstream to upstream for each glacier. The flowlines of AVA predominantly converge on the western side of the basin because AVA is formed by the confluence of two upstream tributaries, and we focus on the main tributaries with higher velocities on the western side. RNK has eight flowlines because half of the terminus region of this glacier is floating (Medrzycka et al., 2016) and we want to examine the velocity variations of the floating and grounded ice separately. We identify floating ice based on the flattening of the surface elevation along flowlines towards the terminus and we take the mean of the velocities on floating ice and grounded ice separately (Figure S1). Note that this separation serves as a theoretical experiment designed to assess the potential impact of surface slope on simulated velocity. We refrain from employing bed elevation data to ascertain the floating condition for RNK because of the reliance of the bed data on mass conservation and the assumption that the glacier is grounded (Morlighem et al., 2017). Terminus position data come from AutoTerm (Zhang et al., 2023), a machine learning pipeline that automatically produces terminus traces with an average sampling frequency of 10 per month since 2014. We derive a time series of terminus changes by calculating the sequential area changes between termini, accumulating these over time, and then normalizing this by a static glacier width of 4.6 km for RNK, 6 km for AVA, 5 km for KUJ, 4 km for KAN, and 3 km for EQP.

We generate surface elevation data through a novel fusion of ICESat-2 data with DigitalGlobe high-resolution digital elevation models (DEM), termed "DG-IS2-DEM" producing four DEMs per year since Fall 2018. The algorithms that generate the DG-IS2-DEMs are described in the Supplementary Information. We also use ArcticDEM (Porter et al., 2022) as supplementary elevation data in locations where the DG-IS2-DEMs do not extend to the most advanced terminus position found in AutoTerm. To determine ice thickness, we subtract surface elevation data from bed elevation data from BedMachineV5 (Morlighem et al., 2022), which assimilates seafloor bathymetry and ice thickness data through a mass conservation approach (Morlighem et al., 2017). We extract the surface and bed elevation profiles along each flowline individually. We use GSFC-FDMv1.2.1 simulations of the surface mass balance (Medley et al., 2022) to produce a runoff time series with a five-day sampling frequency. We use runoff as a proxy for the start and end of the melt season.

4 Terminus-Driven model

Force balance methods can be used to understand the dynamic evolution of glaciers through examination of the balance of stresses on them (Veen et al., 2011; Carnahan et al., 2022). However, the force balance method requires double derivative of surface velocity data, which can result in large uncertainties when using satellite products that have lower accuracy including ITS_LIVE. Therefore, we adopt a different approach that employs a modified force balance termed the "terminus-driven model" described by Joughin et al. (2012). This model explicitly considers the influence of the dynamic changes at the glacier terminus on upstream velocity. By using the terminus-driven model and near daily velocity data, we are able to isolate the contribution of sub-annual terminus variations to the observed variations in the velocity time series. The terminus-driven model is a 1-D model along the flow direction, assuming both an ice mélange free condition and a consistent glacier geometry over time. Additionally, since we use a consistent bed elevation product in our model, we assume that all the glaciers are grounded and that the elevation does not change over time. The terminus-driven model focuses on the driving stress (τ_d) expressed as

$$\tau_d = -\rho_i \times gH \times \frac{\partial h}{\partial x} \tag{1}$$

where g is the gravitational acceleration, H is ice thickness, h is ice surface elevation, and ρ_i is the density of ice (910 km/m^3). In addition, the terminus driven model examines an additional force due to the presence of the free calving face. This latter force is determined by the height above the fjord surface at the calving front and the density of seawater. The difference between these two forces at the terminus is expressed as

$$F = \frac{1}{2} \times \rho_i \; gH^2 - \frac{1}{2} \times \rho_w \; g(H-h)^2 \tag{2}$$

where ρ_w is the density of seawater (1028 km/m^3). Here, we call F the "frontal force" following the naming convention found in Joughin et al. (2012), although it has units of N/m. The force balance at the terminus requires the frontal force to be balanced upstream by the longitudinal stress, which redistributes much of the frontal force to the margins and bed of the glacier upstream. We term the longitudinal stress that originates from the frontal force as $\tau_F(X)$, which pulls the glacier and enhances the original driving stress (e.g., $\tau_d + \tau_F(X)$).

The integration of $\tau_F(X)$ along the flowline equals F and is assumed to linearly decrease upstream of the terminus to zero at the stress coupling length following Joughin et al. (2012):

$$\tau_F(X) = 2 \times \frac{F}{\lambda} \times (1 - \frac{X}{\lambda}) \tag{3}$$

where λ is the stress coupling length, and X is the distance between terminus and the point where we simulate velocity. The terminus variations cause changes in the geometry of the free calving, consequently influencing the frontal force (F). These changes in the frontal force, subsequently, lead to modifications in the enhanced driving stress ($\tau_d + \tau_F(X)$) in the upstream region.

In the lamellar flow model or the shallow ice approximation, when basal sliding is zero, the surface velocity has a linear relationship with the cube of driving stress (n=3) (Van der Veen, 2013):

$$V = \frac{1}{2} A H \tau_d^3 \tag{4}$$

where A is a constant from Glen's flow law. Such a linear relationship also applies when the driving stress is mainly balanced by lateral drag (Van der Veen, 2013):

$$V = \frac{1}{2} A (\frac{\tau_d}{H})^3 W^4 \tag{5}$$

where W is half of the glacier width. Based on the above two models and following the method designed by Joughin et al. (2012), we assume a linear relationship between velocity and the cube of the enhanced driving stress: $\tau_d + \tau_F(X)$, and the predicted velocity from terminus changes is thus given by:

$$\frac{V\,(X,t)}{V_0} = \left(\frac{\tau_d + \tau_F(X)}{\tau_d + \tau_{F_0}} \right)^3 \tag{6}$$

where V_0 is a reference velocity at the same location as velocity observations and τ_{F_0} is the $\tau_F(X)$ corresponding to the reference velocity. For each year, we use the minimum velocity observation as the reference velocity (following Joughin et al. (2012) and calculate τ_{F_0} based on the terminus position nearest the date of the reference velocity. Using Eqn. 6, we can simulate a velocity time series at each observation point for each glacier (Figure 1).

We vary stress coupling lengths for each glacier and choose the one that produces the lowest mean difference between observations and simulated velocity (Table S1). The mean difference is determined by:

$$\frac{abs(model - observation)}{model} \times 100\% \tag{7}$$

For each flowline, we extract the geometry profile and compute a simulated velocity and then average the simulated velocity across all flowlines in a manner consistent with observed velocity. Subsequently, we compare these averaged simulated velocities to observed velocities.

Although the terminus-driven model was initially designed by Joughin et al. (2012) to assume invariant geometry in its operation, we analytically examine the impact of seasonal variations in surface elevation on velocity simulations. Specifically, we leverage the new time-varying DG-IS2-DEM and periodically update the elevation profiles each quarter from Fall 2018, maintaining profile consistency within each quarter. We produce a simulated velocity for all glaciers with and without time-varying surface elevation in order to evaluate the impact of seasonally-varying surface elevation change on velocity. For the fixed geometry simulations, we choose a time step from DG-IS2-DEM with an extent that aligns best with the position of the terminus when it is most advanced. This provides the most complete elevation profile across the terminus region. For EQP, KAN, and AVA we choose the October 2019 DG-IS2-DEM and for KUJ, we use the April 2019 DG-IS2-DEM time step. For RNK, we use additional elevation data from ArcticDEM (Porter et al., 2022) for the fixed geometry case, as the DG-IS2-DEM does not cover the most advanced terminus position for this glacier.

5 Results

5.1 Comparison between velocity simulation and observations

We compare the simulated velocity time series with velocities from satellite observations to determine whether seasonal velocity variations are influenced primarily by terminus change, co-influenced by other factors, or entirely independent of terminus change. Overall, we find that the time-series velocity observations from 2015 are well-described by the terminus-driven model for the grounded portions of RNK, KUJ, and EQP but not for KAN and AVA (Figures 2-6). For RNK, KUJ, and EQP, seasonal changes in glacier speed align well with terminus variations. This is supported by the coincident timing of the end of terminus retreat and the peak summertime velocity (vertical black lines in Figure 2, 4, and 6), even in instances when retreat continues beyond the end of the melt season (Figure 6). For these glaciers, the mean misfit between simulated and observed velocities over all years are 4.6% for KUJ, 6.2% for EQP, and 6.8% for RNK (Table S1), with correlations of 0.84, 0.67, and 0.56, respectively (Figure 7).

For AVA and KAN, we find that simulated velocities differ substantially from the observed velocities. For AVA, simulated velocity fluctuations are relatively small in magnitude compared to observations (Figure 3), while at KAN, the simulated and observed velocities are out of phase but of the same magnitude (Figure 5).

5.2 Compounded velocity processes

Although the terminus-driven model adequately resolves seasonal variability in velocity for RNK, KUJ, and EQP, there are observed sub-seasonal velocity changes that are not explained by the terminus-driven model alone. For all glaciers but KUJ, we observe additional pulses in velocity (acceleration and deceleration) in the middle of the melt season, a phenomenon not captured by the terminus-driven model (black dashed boxes in Figure 2,3,5, and 6). Especially for EQP, the acceleration induced by terminus changes, along with melt-season pulses, collectively form a bimodal velocity response. While these are predominant, they do not as obviously across all years for all glaciers. For example, melt-season pulses are strongly visible for every year in the record for AVA (Figure 2) but they are only obviously visible from 2015-2019 for KAN (Figure 5). For 2020 and 2021 the change in velocity in the melt season is less prominent. Similar for EQP for 2020 and 2021 the melt season pulses are less obvious (Figure 6). Melt season pulses for RNK are even more sporadic (Figure 2).

In addition to melt-season velocity pulses, we find additional sub-seasonal pulses on RNK that coincide with large calving events. RNK experiences much larger calving events than the other glaciers and these create large ($\sim$1 km) step changes in the terminus position. Calving-related pulses in velocity are only predicted to impact velocity noticeably for the grounded portion of RNK (Figure 2d). While we observe sub-seasonal velocity pulses that are coincident with some of these predicted events (blue dashed box in Figures 2), they have a magnitude that is muted compared to those predicted by the terminus-driven model. Further, there are many more predicted velocity pulses from large calving events than are visible in the observed velocity.

While both KAN and AVA experience summertime terminus retreat and wintertime terminus advance similar to the other three glaciers, their velocity response is poorly predicted by the terminus-driven model. For these two glaciers, we observe accelerations during winter (during terminus advance) that plateau before the onset of the melt season in the following year, and early melt season accelerations with the annual maximum velocity reached in the middle of the melt season (black dashed boxed in Figures 3 and 5). The terminus-driven model does not capture wintertime acceleration because across all glaciers the terminus is advancing in winter. For KAN, the model predicts slight deceleration in winter (Figure 5). For AVA, there is no significant seasonality in the simulated velocity likely because the scale of seasonal terminus advance and retreat for this glacier is small (Figure 3) and the surface elevation is flat in frontal region (Figure 8). For reference the averaged seasonal range in terminus position is 144 meters for AVA, while EQP is 224 meters, KAN is 390 meters, and KUJ is 417 meters.

5.3 Experiments with seasonally varying surface elevation

We investigate the influence of changing surface topography by comparing the velocity simulated using a fixed geometry against velocity simulated using a seasonally varying surface elevation from 2018-2022. We find minimal differences between these results for all glaciers (black versus red lines in Figure 3–6). To investigate this further, we consider only KUJ as an example and probe the terminus-driven model via two experiments; 1) we artificially shift the entire elevation profile vertically by $\pm$10-20 meters and; 2) we alter the surface slope by $\pm 2\%$ within the 2 km-frontal region. The results suggest that terminus-driven velocities are relatively insensitive to spatially uniform along-flow changes in surface elevation, but are highly sensitive to changes in surface slope (Figure 9). This result is important for providing context for interpreting the results for RNK, which has a flat, floating portion of the terminus. We find that while the seasonal variations in velocity are similar on the floating and grounded portions of RNK, the simulated velocities in the floating portion are much lower magnitude and lack strong seasonality (Figure 2e).

6 Discussion

6.1 Potential explanations of the compounding seasonality

Using high-temporal-resolution observations and a terminus-driven model to simulate velocity variations from terminus change, we investigate sub-seasonal velocity changes for GrIS outlet glaciers and find that glacier velocity responds to multiple compounding processes. The seasonal velocity changes of three glaciers (KUJ, EQP, and the grounded portion of RNK) can largely be attributed to seasonal terminus variation, particularly for KUJ, which has a velocity that is almost entirely driven by the terminus fluctuations. However, four out of our five study glaciers experience additional processes that drive changes in velocity. EQP, RNK, AVA, and KAN all experience occasional sub-seasonal peaks in velocity that are coincident with the middle of the melt season, AVA and KAN exhibit wintertime speedup that occurs when their termini are advancing, and RNK experiences short-time pulses in velocity throughout the record.

We hypothesize that the peaks in the middle of the melt season observed for EQP, RNK, AVA, and KAN (black dashed squares in Figure 2,3,5, and 6) result from runoff-driven acceleration and subsequent evolution of the subglacial drainage system (Moon et al., 2014; Vijay et al., 2019). Early in the melt season, the subglacial drainage system is inefficient (Andrews et al., 2014), thus as meltwater availability begins to increase (marked by increasing runoff in early summer), subglacial water pressures increase enhancing basal sliding by reducing friction between the ice and the bed (Bartholomew et al., 2010; Bartholomaus et al., 2008). As the melt season progresses, the drainage system channelizes becoming more efficient (Andrews et al., 2014; Schoof, 2010) and available meltwater decreases, producing a reduction in glacier speed. Beyond the melt season, the impact of terminus retreat on seasonal velocities can become more pronounced. For example, EQP typically has a melt season that ends in October, but the terminus continues to retreat until December/January (Figure 6). This produces a wintertime peak in velocity that is coincident with the most retreated terminus of EQP and is distinct from the melt-season peak.

To further explore the velocity increases that occur in summer we examine the along-flow variability in velocity to determine how far upstream velocity changes occur (Figure 10). We extract along-flow velocity profiles from monthly velocity mosaics provided by the the Greenland Ice sheet Mapping Project (Joughin, 2023). We use this dataset only for extracting velocity profiles, specifically to achieve better spatial consistency. To confirm that runoff drives summertime speed up for EQP, we compare the along-flow spatial pattern of velocity change that occurs in the summer melt season of 2017 (Apr 2017 - Sep 2017; Figure 10a) and the subsequent time period after runoff has ceased, when the velocity is primarily influenced by terminus changes (Oct 2017 - Mar 2018; Figure 10b). We quantify the range of upstream velocity at a distance of 10 km upstream of the terminus, which is 25 times the terminus thickness to ensure we are several longitudinal coupling lengths upstream of the terminus. We find that runoff-driven acceleration is noticeable in the velocity further upstream than during the period of terminus-driven velocity change. For example, when the runoff is large, EQP experiences a range in upstream velocity that is 64% of the velocity range observed at the terminus (Figure 10a). Conversely, in the winter when runoff is absent and the terminus alone is changing, EQP experiences a range in upstream velocity inland that is just 12% of what is observed at the terminus (Figure 10b). The rapid decline in speed with distance from the terminus is expected when a glacier is terminus-driven because of the reduction in the terminus force with distance from the terminus (Joughin et al., 2012). Conversely, elevated inland velocities are typical for melt-driven acceleration (Sundal et al., 2011) because meltwater percolates throughout the entire ablation zone (Andrews et al., 2014), which extends about 700 km inland of the terminus for EQP (Noël et al., 2019).

While AVA and KAN experience mid-summer velocity pulses similar to EQP, they do not exhibit any terminus-driven seasonal acceleration (Figures 3 and 5) and instead accelerate in winter. This suggests a decoupling between velocity changes and terminus change for these glaciers. We examine wintertime acceleration similar to above by determining the along-flow pattern of velocity change (Figure 10c, and d). For both glaciers we find significant inland acceleration. For KAN, the range in upstream velocity during winter is 72% of the range in frontal velocity and for AVA, the range in upstream velocity is 39% of the range of frontal velocity, which is larger than terminus-driven upstream velocity range that was observed for EQP (Figure 10c and d versus b). We hypothesize that the elevated range of KAN and AVA's upstream velocities in winter suggests that winter acceleration is due to enhanced extensive basal slip, which can be caused by several different processes. During the onset of winter, refreezing of percolating meltwater (Boon & Sharp, 2003) and viscous deformation over subglacial conduits (Vieli et al., 2004; Bartholomaus et al., 2011) can obstruct the drainage system. Consequently, water becomes trapped within an inefficient drainage network, leading to increased water pressure and winter acceleration (Vijay et al., 2019). There are three possible sources of water at the ice-bed interface during winter: 1) remnants of summer meltwater (Iken & Truffer, 1997), 2) englacial water stored by basal crevasses that do not reach the surface (Abe & Furuya, 2015; Harper et al., 2010), and/or 3) sustained exfiltration of underground water caused by rapid unloading in melt season (Robel et al., 2023). The winter acceleration phase ends when the melt season begins to supply additional water to the subglacial system, which further increases basal water pressures causing summertime pulses in speed forcing the glacier to reach maximum speeds in summer.

RNK is a glacier that experiences three distinct modes of velocity variations including 1) seasonal terminus-driven velocity change; 2) occasional runoff-driven velocity change and; 3) frequent, small-magnitude velocity change that appears to be linked to large calving events. Large calving events have been documented to cause step-like acceleration for Helheim Glacier (Nettles et al., 2008; de Juan et al., 2010) and, like Helheim, RNK experiences calving via buoyant flexure causing glacier-wide step-retreat of the terminus position (Fried et al., 2018; Medrzycka et al., 2016). Calving-related velocity pulses at RNK are significantly muted compared to those predicted by the terminus-driven model. In part, this may be due to the lower sampling frequency of terminus change. Prior to 2017, our terminus record of RNK contains just six termini per month while after 2017, there are up to fourteen termini per month. Indeed, we observe more correlation between the magnitude of velocity pulses related to calving events between the observed and simulated velocities after 2017. In addition to reduced sampling frequency, the floating portion of RNK with its flat surface topography produces a much weaker simulated velocity pulse in response to calving events than is seen on grounded ice, where surface topography is much steeper. Thus, the floating ice with its flat surface topography dampens the impact of calving on surface speed.

The floating portion of the RNK terminus produces simulated velocities that have a much lower magnitude than observed (Figure 2), indicating that velocity change on this part of RNK is not driven by terminus change through longitudinal stress coupling. Terminus change may still have a strong, but more indirect impact on the velocity change on the floating portion via lateral stresses originating on the adjacent grounded ice. In contrast, the observed velocities in the floating portion of RNK show just as much variation over time as we observe in the grounded portion. We attribute this discrepancy to the fact that the terminus-driven model captures longitudinal stresses but not lateral stresses. Thus, the seasonal variations in the observed velocity over the floating region might be driven by the nearby velocities on the grounded ice through lateral stress, which is not captured by the terminus-driven model. The impact of flotation may also be observed on the grounded ice. For example, in 2017 and 2018 RNK underwent a large multi-year advance ($\sim$ 1000 meters), after which the seasonal variations in both simulated and observed velocity in the grounded ice are reduced in amplitude compared to other years.

We speculate that as the glacier advanced, its original grounded front became floating and the surface flattened, which caused the velocity to be less sensitive to seasonal terminus variation.

6.2 Impact of observed seasonal elevation changes

The availability of seasonally-resolved elevation change allows us to investigate the degree to which velocity is sensitive to changing surface elevation. We find that seasonal elevation change for EQP, KAN, KUJ, and AVA is relatively uniform along flow (Figure 8), and as a result, they do not significantly alter terminus-driven velocity (black lines in Figures 3–6). This aligns with our experimental results that suggest that vertical shifts in elevation have a limited contribution to velocity seasonality (Figure 9a). The experimental results also suggest steepening surface elevation will cause stronger velocity responses (Figure 9b), which agrees with our results for RNK that simulated velocity is comparable with observations along the steep grounded flowlines but nearly absent on flat floating flowlines (Figure 2).

6.3 Analysis of model sensitivity on velocity positions and derived stress coupling lengths

We further test the sensitivity of the position of the velocity points to the results by including more data points in both upstream and downstream regions (blue points in Figure 1). For RNK, KUJ, and EQP, differences exist between upstream and downstream measurements (Figures S2, S3, S5, S7). The spatial changes for AVA and KAN in both velocity observations and simulations are subtle (Figures S4 and S6). However, the temporal pattern of velocity remains relatively consistent across the entire watershed, with only the magnitude of velocity decreasing from downstream to upstream. In the ground portion of RNK, both observed and simulated velocity exhibit reduced seasonality from downstream to upstream, while also displaying a clear calving-induced acceleration. While most regions of the floating portion exhibit no discernible seasonality in the simulations, some areas demonstrate moderate seasonality (Figures S3b and S3c). The moderate seasonality of these areas can be attributed to their relatively small driving stress; when the driving stress is reduced, the impact of $\tau_F(X)$ on velocity becomes more pronounced.

Our simulated velocities match well with the observed ones for KUJ and EQP overall. However, the simulated velocity for KUJ overestimates the seasonality in 2020 in upstream regions (Figures S5e and f) and underestimates the seasonality in 2021 in downstream regions (Figure S5). This suggests that environmental factors, aside from terminus change, may influence the seasonality of velocity for KUJ, and that this influence varies spatiotemporally. In 2020, seasonal elevation change in EQP diminish the simulated velocity's seasonality more prominently in the upstream region, better aligning with observed velocity than in the downstream region (Figures S7d and e). However, the terminus-driven model with varying geometry overestimates the seasonal velocity in the downstream region. We hypothesize that seasonal elevation change acts to dampen the seasonal velocity signal in the upstream region, potentially propagating downstream. However, since the terminus-driven model only considers the geometry at a given location, it thus fails to capture such propagation.

The stress coupling length is 25km for RNK, 10km for EQP, and 20km for KUJ (Table S1). KAN and AVA's seasonal velocities are not driven by terminus variation, so we do not include the estimation of stress coupling length for these glaciers. Enderlin et al. (2016) estimated the stress coupling length by using an empirical method, suggesting that the stress coupling length should be approximately four times the glacier thickness, which is smaller than our estimation. Our estimation of SCL might be uncertain since we assume a constant stress coupling length along the profile and the terminus-driven model is a simplified 1-D model.

7 Conclusion

We apply a terminus-driven model to elucidate the seasonal and sub-seasonal velocity changes for five glaciers in Central West Greenland. The comparison between simulated and observed velocity suggests that glacier velocity change is driven by the interplay of multiple processes: terminus variations, runoff changes, evolution of the subglacial drainage system, and calving. Most glaciers exhibit more than one of these velocity variations and thus are a compounded signal. Notably, the observed seasonal elevation changes appear to have limited influence on simulated velocities largely because the seasonal elevation signal is dominated by shifts in elevation and not changes in surface slope. Our experiments indicate that changes in surface slope have a stronger impact on the response of velocity to terminus changes than uniform changes in elevation. Our study provides a framework that can be applied to all outlet glaciers around the Greenland Ice Sheet to reveal the compounded nature of each glacier's seasonal velocity change. Moreover, the same framework could be applied to investigate the long-term changes in glacier dynamics with adequate historical data. By systematically discerning the commonalities and disparities among glaciers with distinct glaciological settings, our approach has the potential to shed light on diverging controls on outlet glaciers.

Acknowledgments

We acknowledge funding for this work from NASA (Grant NNH20ZDA001N-ICESAT2) and the Institute for Geophysics Postdoctoral Fellowship at the Jackson School to E. Zhang. We acknowledge the National Snow and Ice Data Center QGreenland package (Moon et al., 2023). We acknowledge DEMs provided by the Polar Geospatial Center under NSF-OPP awards 1043681, 1559691, 1542736, 1810976, and 2129685.

References

Abe, T., & Furuya, M. (2015). Winter speed-up of quiescent surge-type glaciers in yukon, canada. *The Cryosphere*, *9*(3), 1183–1190. doi: 10.5194/tc-9-1183-2015

Andrews, L. C., Catania, G. A., Hoffman, M. J., Gulley, J. D., Lüthi, M. P., Ryser, C., ... Neumann, T. A. (2014). Direct observations of evolving subglacial drainage beneath the greenland ice sheet. *Nature*, *514*(7520), 80–83. doi: 10.1038/nature13796

Bartholomaus, T. C., Anderson, R. S., & Anderson, S. P. (2008). Response of glacier basal motion to transient water storage. *Nature Geoscience*, *1*(1), 33–37. doi: 10.1038/ngeo.2007.52

Bartholomaus, T. C., Anderson, R. S., & Anderson, S. P. (2011). Growth and collapse of the distributed subglacial hydrologic system of kennicott glacier, alaska, usa, and its effects on basal motion. *Journal of Glaciology*, *57*(206), 985–1002. doi: 10.3189/002214311798843269

Bartholomew, I., Nienow, P., Mair, D., Hubbard, A., King, M. A., & Sole, A. (2010). Seasonal evolution of subglacial drainage and acceleration in a greenland outlet glacier. *Nature Geoscience*, *3*(6), 408–411. doi: 10.1038/ngeo863

Boon, S., & Sharp, M. (2003). The role of hydrologically-driven ice fracture in drainage system evolution on an arctic glacier. *Geophysical Research Letters*, *30*(18). doi: https://doi.org/10.1029/2003GL018034

Carnahan, E., Catania, G., & Bartholomaus, T. C. (2022). Observed mechanism for sustained glacier retreat and acceleration in response to ocean warming around Greenland. *The Cryosphere*, *16*(10), 4305–4317. doi: 10.5194/tc-16-4305-2022

Catania, G. A., Stearns, L. A., Sutherland, D. A., Fried, M. J., Bartholomaus, T. C., Morlighem, M., ... Nash, J. (2018). Geometric controls on tidewater glacier retreat in central western Greenland. *Journal of Geophysical Research: Earth Surface*, *123*(8), 2024-2038. doi: 10.1029/2017JF004499

Davison, B. J., Sole, A. J., Cowton, T. R., Lea, J. M., Slater, D. A., Fahrner, D., & Nienow, P. W. (2020). Subglacial drainage evolution modulates seasonal ice flow variability of three tidewater glaciers in southwest greenland. *Journal of Geophysical Research: Earth Surface*, *125*(9), e2019JF005492. doi: https://doi.org/10.1029/2019JF005492

de Juan, J., Elósegui, P., Nettles, M., Larsen, T. B., Davis, J. L., Hamilton, G. S., ... Forsberg, R. (2010). Sudden increase in tidal response linked to calving and acceleration at a large greenland outlet glacier. *Geophysical Research Letters*, *37*(12), L12501. doi: https://doi.org/10.1029/2010GL043289

Enderlin, E. M., Hamilton, G. S., O'Neel, S., Bartholomaus, T. C., Morlighem, M., & Holt, J. W. (2016). An empirical approach for estimating stress-coupling lengths for marine-terminating glaciers. *Frontiers in Earth Science*, *4*, 104. doi: 10.3389/feart.2016.00104

Enderlin, E. M., Howat, I. M., Jeong, S., Noh, M.-J., van Angelen, J. H., & van den Broeke, M. R. (2014). An improved mass budget for the Greenland ice sheet. *Geophysical Research Letters*, *41*(3), 866-872. doi: 10.1002/2013GL059010

Felikson, D., A. Catania, G., Bartholomaus, T. C., Morlighem, M., & Noël, B. P. Y. (2021). Steep glacier bed knickpoints mitigate inland thinning in greenland. *Geophysical Research Letters*, *48*(2), e2020GL090112. doi: https://doi.org/10.1029/2020GL090112

Felikson, D., Nowicki, S., Nias, I., Morlighem, M., & Seroussi, H. (2022). Seasonal tidewater glacier terminus oscillations bias multi-decadal projections of ice mass change. *Journal of Geophysical Research: Earth Surface*, *127*(2), e2021JF006249. doi: https://doi.org/10.1029/2021JF006249

Fried, M. J., Catania, G. A., Stearns, L. A., Sutherland, D. A., Bartholomaus, T. C., Shroyer, E., & Nash, J. (2018). Reconciling Drivers of Seasonal Terminus Advance and Retreat at 13 Central West Greenland Tidewater Glaciers. *Journal of Geophysical Research: Earth Surface*, *123*(7), 1590-1607. doi: 10.1029/2018JF004628

Gardner, A. S., Fahnestock, M. A., & Scambos, T. A. (2023). *ITS_LIVE regional glacier and ice sheet surface velocities: Version 1.* National Snow and Ice Data Center. Retrieved from `https://doi:10.5067/6II6VW8LLWJ7`

Gardner, A. S., Moholdt, G., Scambos, T., Fahnstock, M., Ligtenberg, S., van den Broeke, M., & Nilsson, J. (2018). Increased west antarctic and unchanged east antarctic ice discharge over the last 7 years. *The Cryosphere*, *12*(2), 521–547. doi: 10.5194/tc-12-521-2018

Goliber, S., Black, T., Catania, G., Lea, J. M., Olsen, H., Cheng, D., ... Zhang, E. (2022). Termpicks: a century of greenland glacier terminus data for use in scientific and machine learning applications. *The Cryosphere*, *16*(8), 3215–3233. doi: 10.5194/tc-16-3215-2022

Harper, J. T., Bradford, J. H., Humphrey, N. F., & Meierbachtol, T. W. (2010). Vertical extension of the subglacial drainage system into basal crevasses. *Nature*, *467*(7315), 579–582. doi: 10.1038/nature09398

Holland, D. M., Thomas, R. H., De Young, B., Ribergaard, M. H., & Lyberth, B. (2008). Acceleration of Jakobshavn Isbræ triggered by warm subsurface ocean waters. *Nature geoscience*, *1*(10), 659–664. doi: 10.1038/ngeo316

Howat, I. M., Joughin, I., Fahnestock, M., Smith, B. E., & Scambos, T. A. (2008). Synchronous retreat and acceleration of southeast Greenland outlet glaciers 2000–06: ice dynamics and coupling to climate. *Journal of Glaciology*, *54*(187), 646–660. doi: 10.3189/002214308786570908

Howat, I. M., Joughin, I., Tulaczyk, S., & Gogineni, S. (2005). Rapid retreat and acceleration of Helheim Glacier, east Greenland. *Geophysical Research Letters*, *32*(22), L22502. doi: 10.1029/2005GL024737

Iken, A., & Truffer, M. (1997). The relationship between subglacial water pressure and velocity of findelengletscher, switzerland, during its advance and retreat. *Journal of Glaciology*, *43*(144), 328–338. doi: 10.3189/S0022143000003282

IPCC. (2022). *Climate change 2022: Mitigation of climate change* (P. Shukla et al., Eds.). Cambridge, UK and New York, NY, USA: Cambridge University Press. doi: 10.1017/9781009157926

Joughin, I. (2023). *Measures greenland monthly ice sheet velocity mosaics from sar and landsat, version 5.* NASA National Snow and Ice Data Center Distributed Active Archive Center. Retrieved from `https://nsidc.org/data/NSIDC-0731/versions/5` doi: 10.5067/EGKZX6FXXM4P

Joughin, I., Das, S. B., King, M. A., Smith, B. E., Howat, I. M., & Moon, T. (2008). Seasonal Speedup Along the Western Flank of the Greenland Ice Sheet. *Science*, *320*(5877), 781–783. doi: 10.1126/science.1153288

Joughin, I., Smith, B. E., Howat, I. M., Floricioiu, D., Alley, R. B., Truffer, M., & Fahnestock, M. (2012). Seasonal to decadal scale variations in the surface velocity of Jakobshavn Isbrae, Greenland: Observation and model-based analysis. *Journal of Geophysical Research: Earth Surface*, *117*(F2), F02030. doi: 10.1029/2011JF002110

Kehrl, L. M., Joughin, I., Shean, D. E., Floricioiu, D., & Krieger, L. (2017). Seasonal and interannual variabilities in terminus position, glacier velocity, and surface elevation at Helheim and Kangerlussuaq Glaciers from 2008 to 2016. *Journal of Geophysical Research: Earth Surface*, *122*(9), 1635-1652. doi: 10.1002/2016JF004133

King, M. D., Howat, I. M., Candela, S. G., Noh, M. J., Jeong, S., Noël, B. P., … Negrete, A. (2020). Dynamic ice loss from the greenland ice sheet driven by sustained glacier retreat. *Communications Earth & Environment*, *1*(1), 1. doi: 10.1038/s43247-020-0001-2

Medley, B., Neumann, T. A., Zwally, H. J., Smith, B. E., & Stevens, C. M. (2022). Simulations of firn processes over the greenland and antarctic ice sheets: 1980–2021. *The Cryosphere*, *16*(10), 3971–4011. doi: 10.5194/tc-16-3971-2022

Medrzycka, D., Benn, D. I., Box, J. E., Copland, L., & Balog, J. (2016). Calving behavior at rink isbræ, west greenland, from time-lapse photos. *Arctic, Antarctic, and Alpine Research*, *48*(2), 263-277. doi: 10.1657/AAAR0015-059

Moon, T., Fisher, M., Stafford, T., & Thurber, A. (2023). *Qgreenland (v3) [dataset].* National Snow and Ice Data Center. Retrieved from `https://10.5281/zenodo.8326507`

Moon, T., Gardner, A., Csatho, B., Parmuzin, I., & Fahnestock, M. (2020). Rapid Reconfiguration of the Greenland Ice Sheet Coastal Margin. *Journal of Geophysical Research: Earth Surface*, *125*(11). doi: 10.1029/2020jf005585

Moon, T., Joughin, I., & Smith, B. (2015). Seasonal to multiyear variability of glacier surface velocity, terminus position, and sea ice/ice mélange in northwest Greenland. *Journal of Geophysical Research: Earth Surface*, *120*(5), 818-833. doi: 10.1002/2015JF003494

Moon, T., Joughin, I., Smith, B., & Howat, I. (2012). 21st-Century evolution of Greenland outlet glacier velocities. *Science*, *336*(6081), 576–578. doi: 10.1126/science.1219985

Moon, T., Joughin, I., Smith, B., van den Broeke, M. R., van de Berg, W. J., Noël, B., & Usher, M. (2014). Distinct patterns of seasonal Greenland glacier velocity. *Geophysical Research Letters*, *41*(20), 7209-7216. doi: 10.1002/2014GL061836

Morlighem, M., Williams, C. N., Rignot, E., An, L., Arndt, J. E., Bamber, J. L., … Zinglersen, K. B. (2017). BedMachine v3: Complete bed topography and ocean bathymetry mapping of Greenland from multibeam echo dounding combined with mass conservation. *Geophysical Research Letters*, *44*(21), 11,051-11,061. doi: 10.1002/2017GL074954

Morlighem, M., Williams, C. N., Rignot, E., An, L., Arndt, J. E., Bamber, J. L., . . . Zinglersen, K. B. (2022). *Icebridge bedmachine greenland, version 5 [data set].* Boulder, Colorado USA. NASA National Snow and Ice Data Center Distributed Active Archive Center. Retrieved from `https://doi.org/10.5067/GMEVBWFLWA7X.DateAccessed08-30-2023.`

Nettles, M., Larsen, T. B., Elósegui, P., Hamilton, G. S., Stearns, L. A., Ahlstrøm, A. P., . . . Forsberg, R. (2008). Step-wise changes in glacier flow speed coincide with calving and glacial earthquakes at helheim glacier, greenland. *Geophysical Research Letters*, *35*(24), L24503. doi: https://doi.org/10.1029/2008GL036127

Noël, B., van de Berg, W. J., Lhermitte, S., & van den Broeke, M. R. (2019). Rapid ablation zone expansion amplifies north greenland mass loss. *Science Advances*, *5*(9), eaaw0123. doi: 10.1126/sciadv.aaw0123

Poinar, K. (2023). Seasonal flow types of glaciers in sermilik fjord, greenland, over 2016–2021. *Journal of Geophysical Research: Earth Surface*, *128*(7), e2022JF006901. doi: https://doi.org/10.1029/2022JF006901

Porter, C., Morin, P., Howat, I. M., Noh, M.-J., Bates, B., Peterman, K., . . . Bojesen, M. (2022). *ArcticDEM - Strips, Version 4.1.* Retrieved 2023, from `https://doi.org/10.7910/DVN/C98DVS`

Rennermalm, A. K., Smith, L. C., Chu, V. W., Box, J. E., Forster, R. R., Van den Broeke, M. R., . . . Moustafa, S. E. (2013). Evidence of meltwater retention within the greenland ice sheet. *The Cryosphere*, *7*(5), 1433–1445. doi: 10.5194/tc-7-1433-2013

Robel, A. A., Sim, S. J., Meyer, C., Siegfried, M. R., & Gustafson, C. D. (2023). Contemporary ice sheet thinning drives subglacial groundwater exfiltration with potential feedbacks on glacier flow. *Science Advances*, *9*(33), eadh3693. doi: 10.1126/sciadv.adh3693

Schoof, C. G. (2010, 12). Ice-sheet acceleration driven by melt supply variability. *Nature*, *468*(7325), 803 806. doi: 10.1038/nature09618

Sergienko, O. V. (2022). Marine outlet glacier dynamics, steady states and steady-state stability. *Journal of Glaciology*, *68*(271), 946–960. doi: 10.1017/jog.2022.13

Shepherd, A., Ivins, E. R., A, G., Barletta, V. R., Bentley, M. J., Bettadpur, S., . . . Zwally, H. J. (2012). A reconciled estimate of ice-sheet mass balance. *Science*, *338*(6111), 1183-1189. doi: 10.1126/science.1228102

Solgaard, A. M., Rapp, D., Noël, B. P. Y., & Hvidberg, C. S. (2022). Seasonal patterns of greenland ice velocity from sentinel-1 sar data linked to runoff. *Geophysical Research Letters*, *49*(24), e2022GL100343. doi: https://doi.org/10.1029/2022GL100343

Stevens, L. A., Nettles, M., Davis, J. L., Creyts, T. T., Kingslake, J., Hewitt, I. J., & Stubblefield, A. (2022). Tidewater-glacier response to supraglacial lake drainage. *Nature Communications*, *13*(1), 6065. doi: 10.1038/s41467-022-33763-2

Sundal, A. V., Shepherd, A., Nienow, P., Hanna, E., Palmer, S., & Huybrechts, P. (2011). Melt-induced speed-up of greenland ice sheet offset by efficient subglacial drainage. *Nature*, *469*(7331), 521–524. doi: 10.1038/nature09740

Ultee, L., Felikson, D., Minchew, B., Stearns, L. A., & Riel, B. (2022). Helheim glacier ice velocity variability responds to runoff and terminus position change at different timescales. *Nature Communications*, *13*(1), 6022. doi: 10.1038/s41467-022-33292-y

van den Broeke, M. R., Enderlin, E. M., Howat, I. M., Kuipers Munneke, P., Noël, B. P. Y., van de Berg, W. J., . . . Wouters, B. (2016). On the recent contribution of the greenland ice sheet to sea level change. *The Cryosphere*, *10*(5),

1933–1946. doi: 10.5194/tc-10-1933-2016
Van der Veen, C. J. (2013). *Fundamentals of glacier dynamics* (Second Edition ed.). New York: CRC press.
Veen, C. J. v. d., Plummer, J., & Stearns, L. A. (2011). Controls on the recent speed-up of Jakobshavn Isbrae, West Greenland. *Journal of Glaciology*, *57*(204), 770 – 782.
Vieli, A., Jania, J., Blatter, H., & Funk, M. (2004). Short-term velocity variations on hansbreen, a tidewater glacier in spitsbergen. *Journal of Glaciology*, *50*(170), 389–398. doi: 10.3189/172756504781829963
Vijay, S., Khan, S. A., Kusk, A., Solgaard, A. M., Moon, T., & Bjørk, A. A. (2019). Resolving seasonal ice velocity of 45 greenlandic glaciers with very high temporal details. *Geophysical Research Letters*, *46*(3), 1485-1495. doi: https://doi.org/10.1029/2018GL081503
Vijay, S., King, M. D., Howat, I. M., Solgaard, A. M., Khan, S. A., & Noël, B. (2021). Greenland ice-sheet wide glacier classification based on two distinct seasonal ice velocity behaviors. *Journal of Glaciology*, *67*(266), 1241–1248. doi: 10.1017/jog.2021.89
Werder, M. A., Hewitt, I. J., Schoof, C. G., & Flowers, G. E. (2013). Modeling channelized and distributed subglacial drainage in two dimensions. *Journal of Geophysical Research: Earth Surface*, *118*(4), 2140-2158. doi: https://doi.org/10.1002/jgrf.20146
Wood, M., Rignot, E., Fenty, I., An, L., Bjørk, A., van den Broeke, M., … others (2021). Ocean forcing drives glacier retreat in greenland. *Science Advances*, *7*(1), eaba7282. doi: 10.1126/sciadv.aba7282
Zhang, E., Catania, G., & Trugman, D. T. (2023). Autoterm: an automated pipeline for glacier terminus extraction using machine learning and a "big data" repository of greenland glacier termini. *The Cryosphere*, *17*(8), 3485–3503. doi: 10.5194/tc-17-3485-2023

Open Research Section

Velocity data can be freely downloaded at `https://its-live.jpl.nasa.gov/` (Gardner et al., 2023). ArcticDEMs are available at `https://livingatlas2.arcgis.com/arcticdemexplorer/`. The code, terminus data, flowlines, and DG-IS2-DEMs can be downloaded at `https://zenodo.org/record/8428196`.

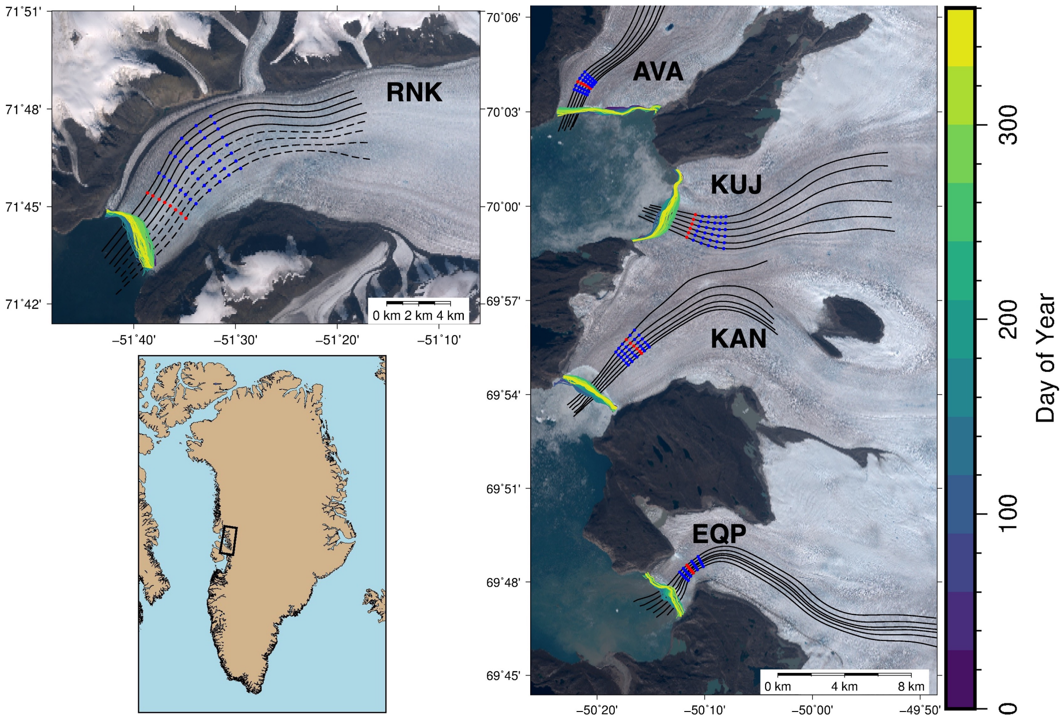

Figure 1. Glacier and data locations. Glaciers examined in this study include Rink Isbrae (RNK), Sermeq Avannarleq (AVA), Sermeq Kujalleq (KUJ), Kangilernata Sermia (KAN), and Eqip Sermia (EQP). Black solid flowlines represent grounded portions of the glaciers while dashed flowlines represent floating portions. The terminus traces in 2018 from AutoTerm are colored by date. Colored points on flowlines are the locations where we obtain velocity time series from ITS_LIVE. The results section shows the results of the red points. Blue points are for testing the sensitivity of the position of velocity to the results.

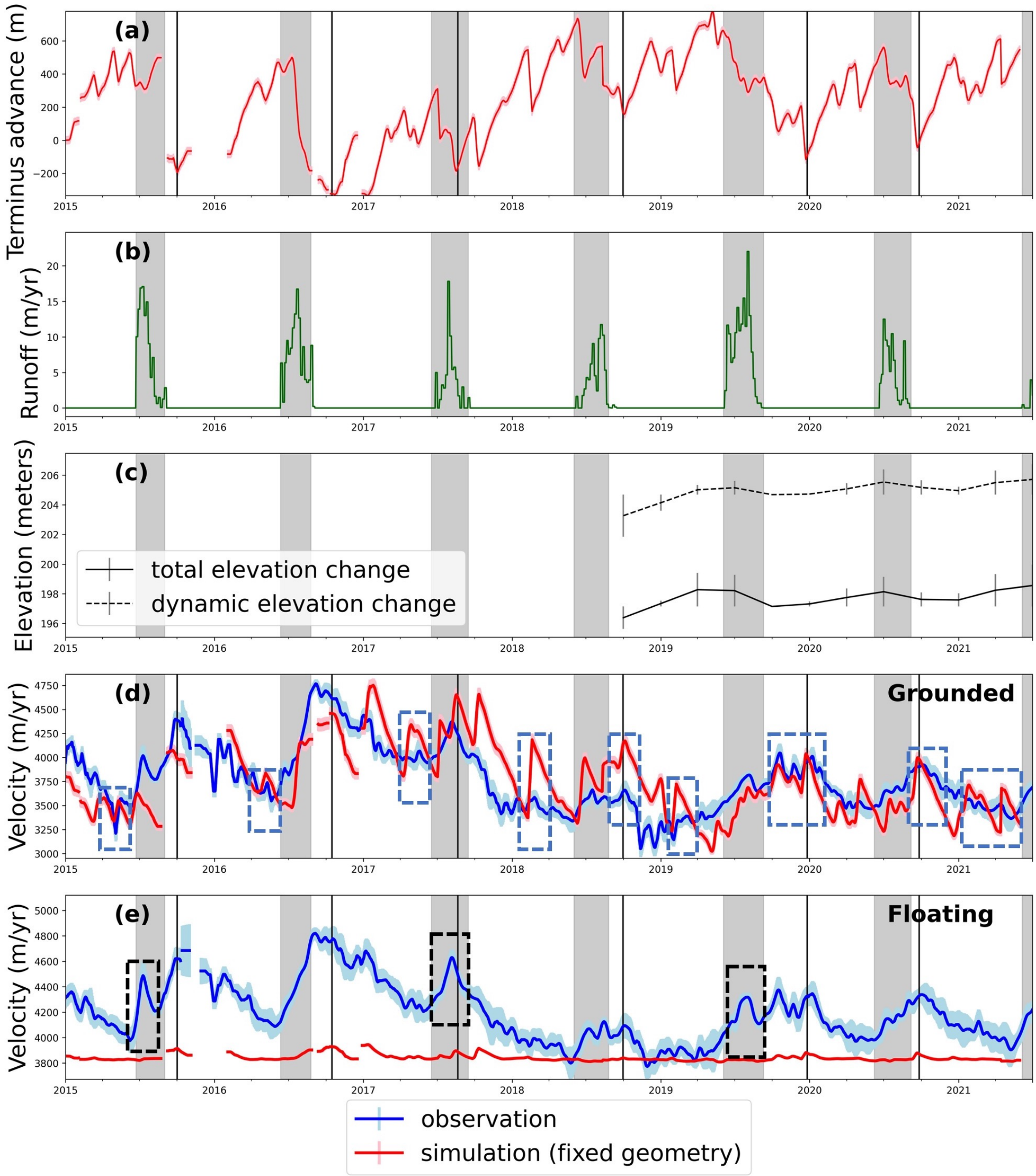

Figure 2. The full record of RNK. (a) is the terminus variation with pink shading representing uncertainty derived from AutoTerm. (b) Displays the runoff time series. (c) Illustrates surface elevation changes. (d) Compares simulated and observed velocity for grounded flowlines. (e) Extends the comparison to floating flowlines (as in d). The dashed boxes show the accelerations caused by runoff.

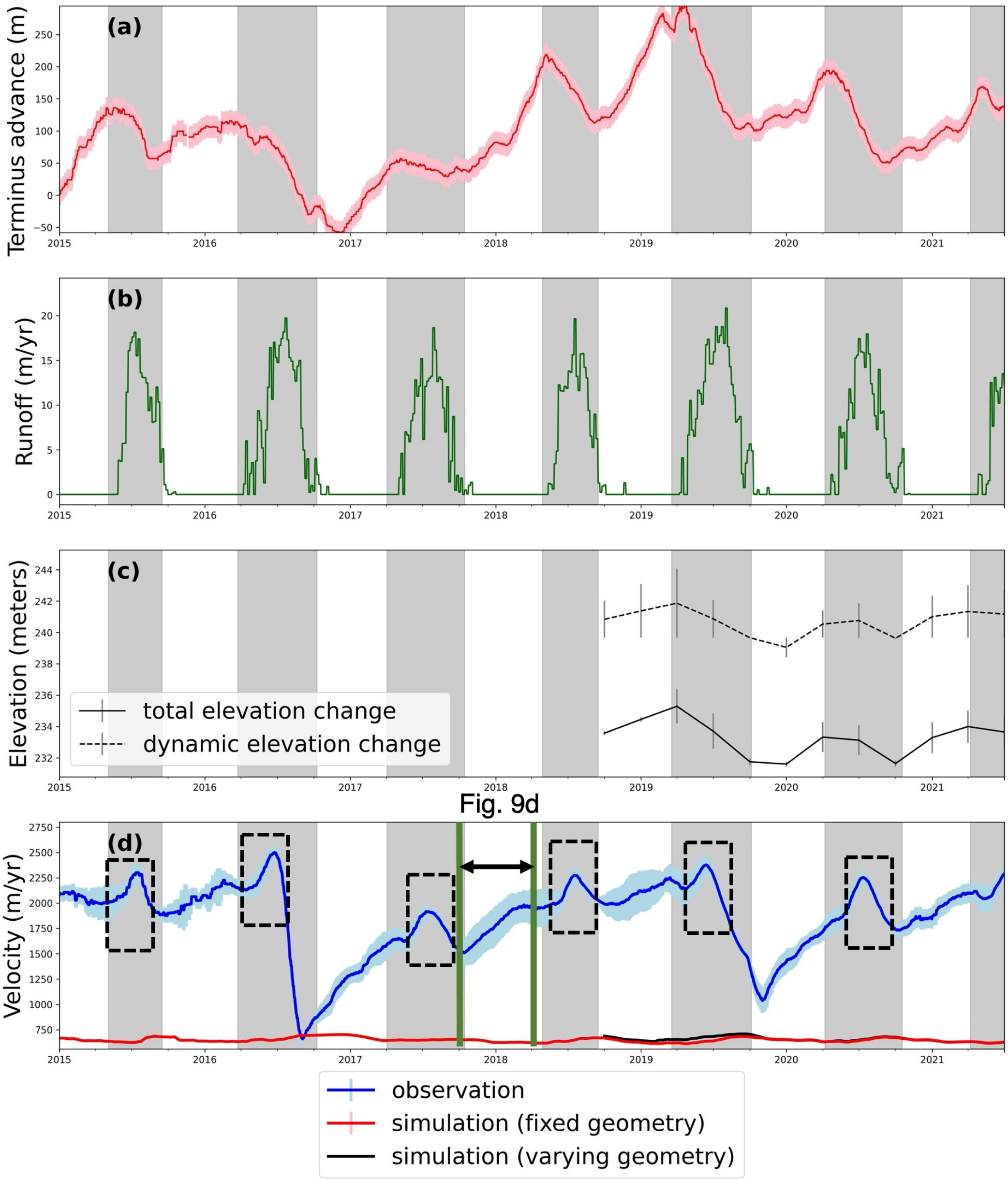

Figure 3. The full record of AVA. The figure follows the same design as Figure 2. The vertical green lines indicate the study period in Figure 10d.

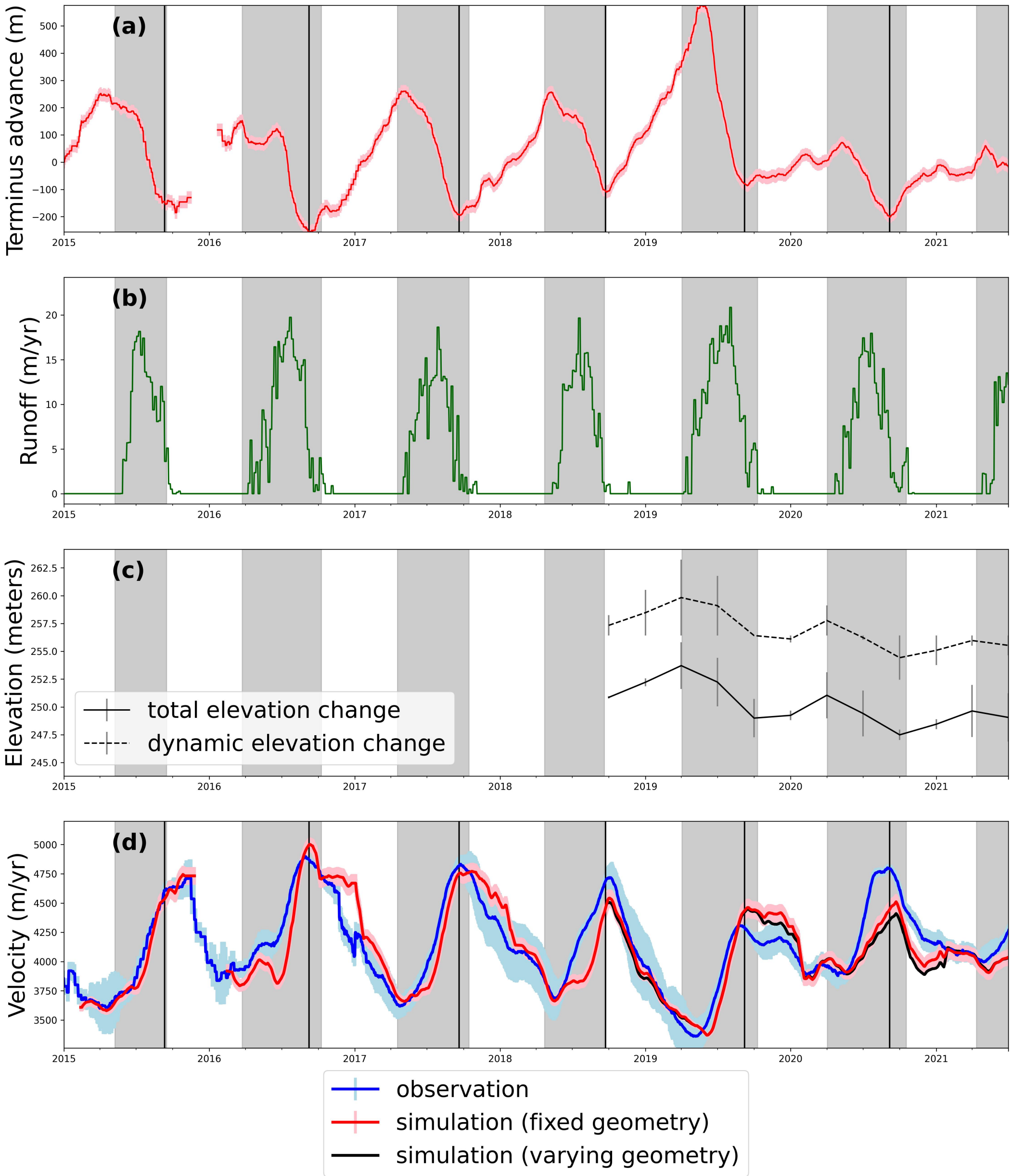

Figure 4. The full record of KUJ. The figure follows the same design as Figure 2.

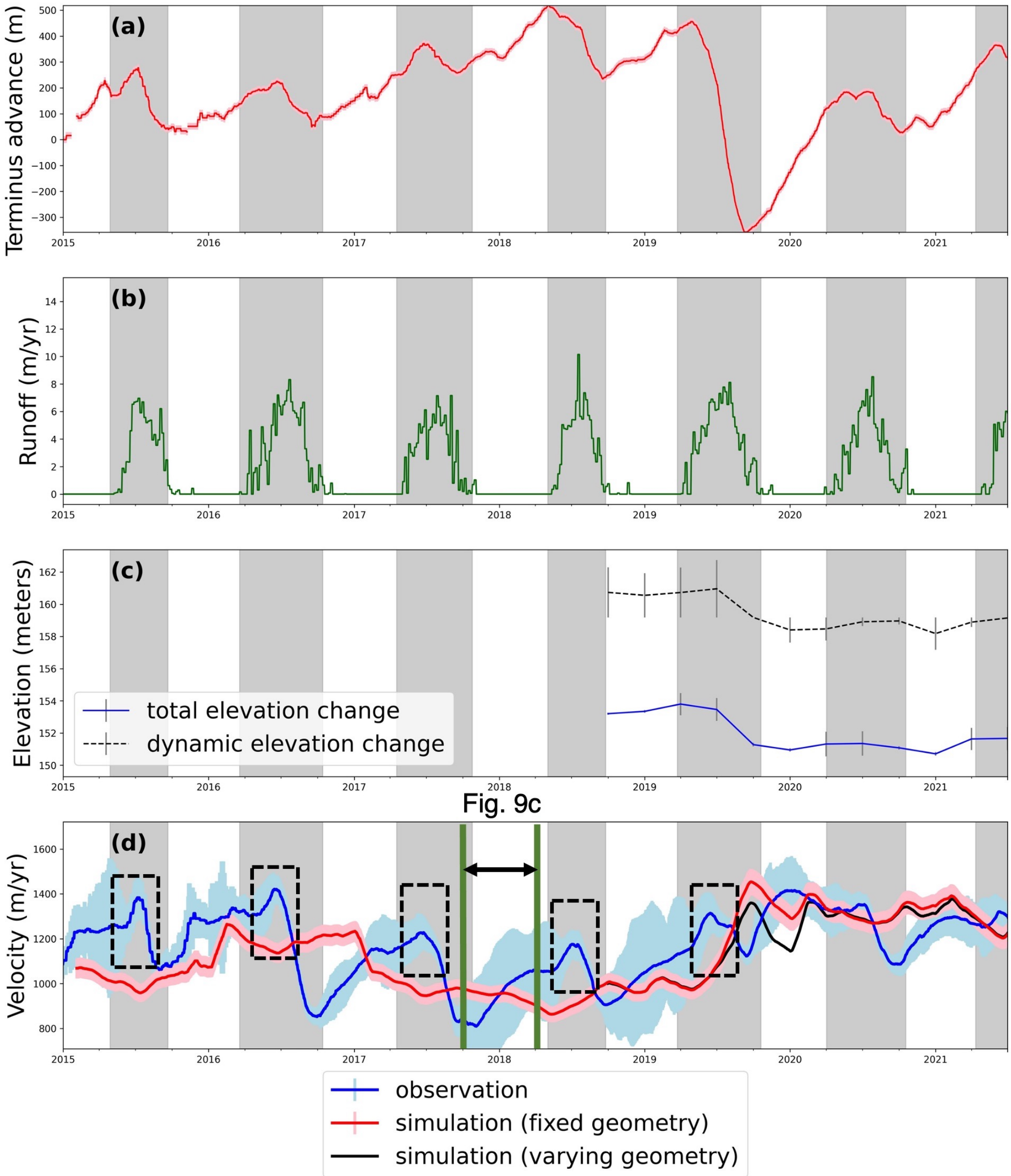

Figure 5. The full record of KAN. The figure follows the same design as Figure 2. The vertical green lines indicate the study period in Figure 10c.

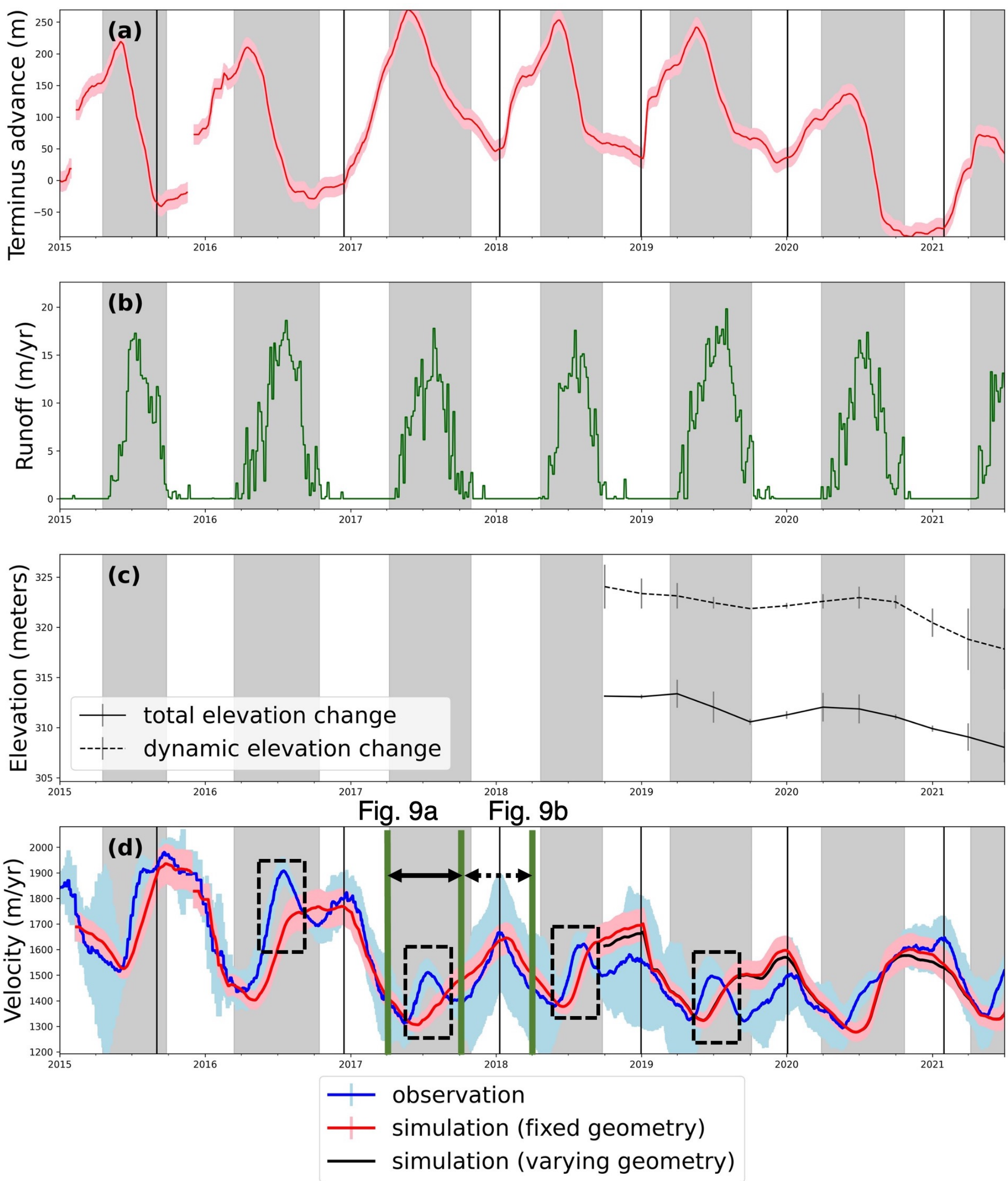

Figure 6. The full record of EQP. The figure follows the same design as Figure 2. The vertical green lines indicate the study period in Figure 10a and 10b.

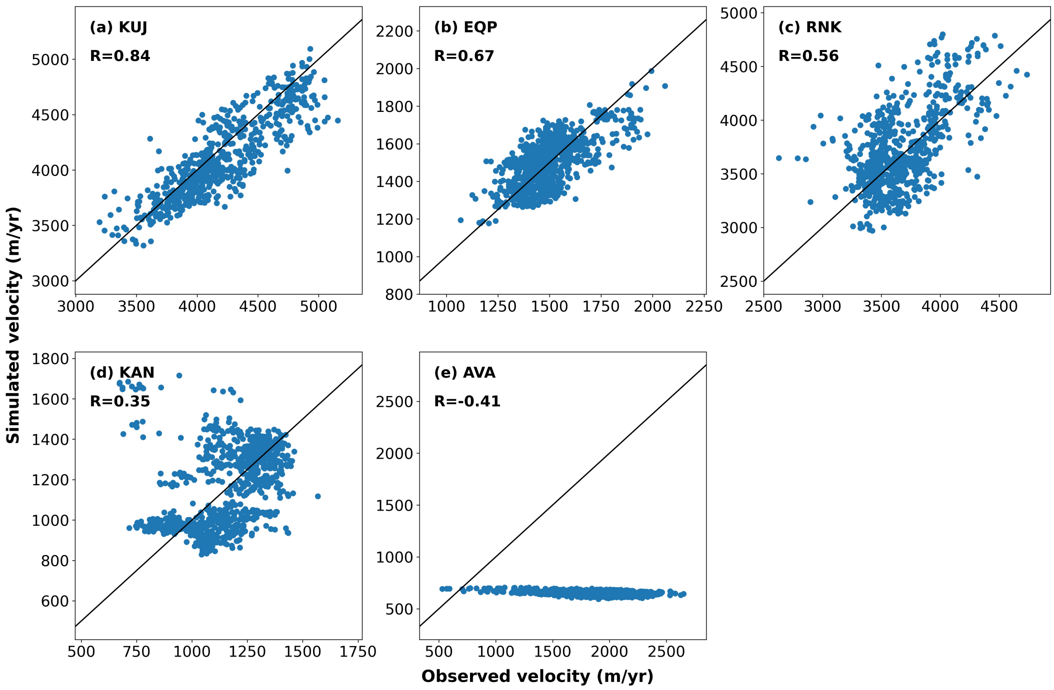

Figure 7. Scatter plot showing the comparison between simulated and observed velocity for KUJ, EQP, RNK, KAN, and AVA. The 1:1 line is as shown for each.

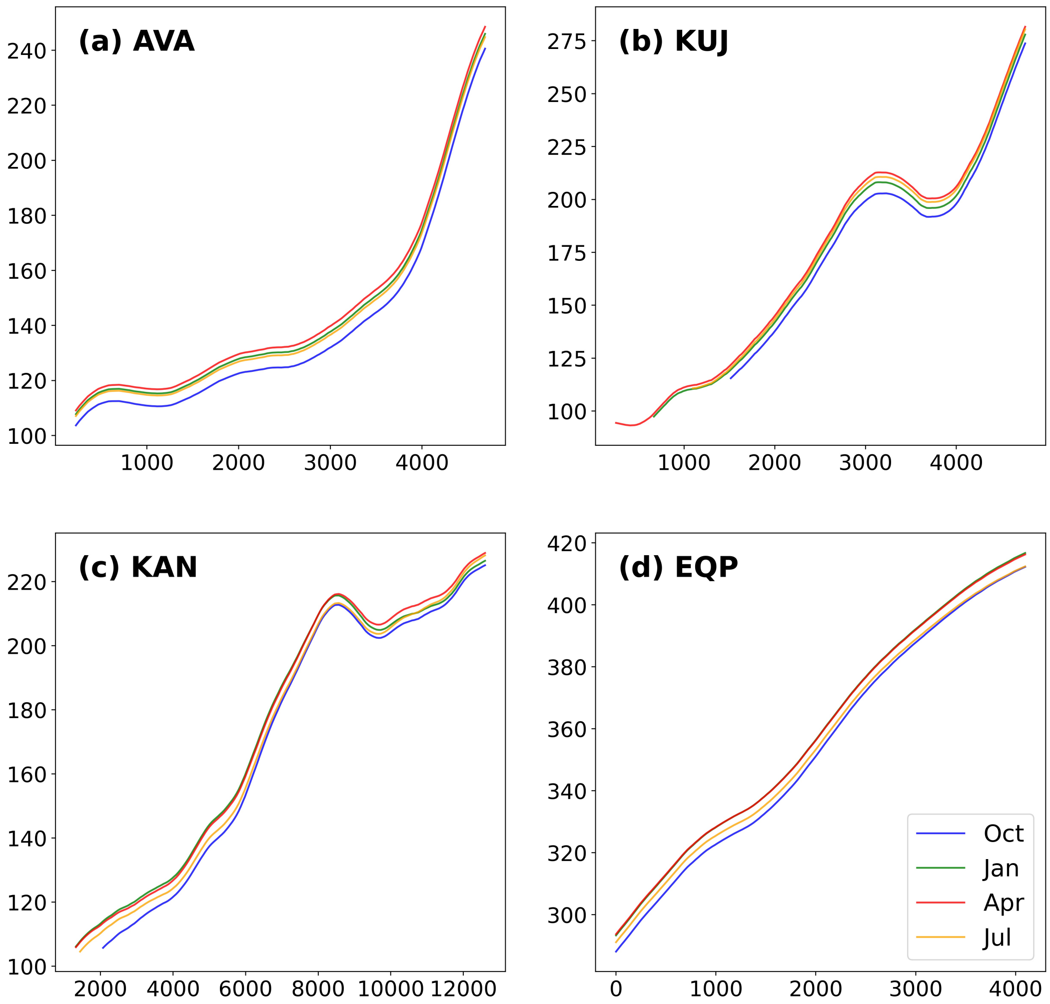

Figure 8. Surface elevation profiles in 2019 for AVA, KUJ, KAN, and EQP.

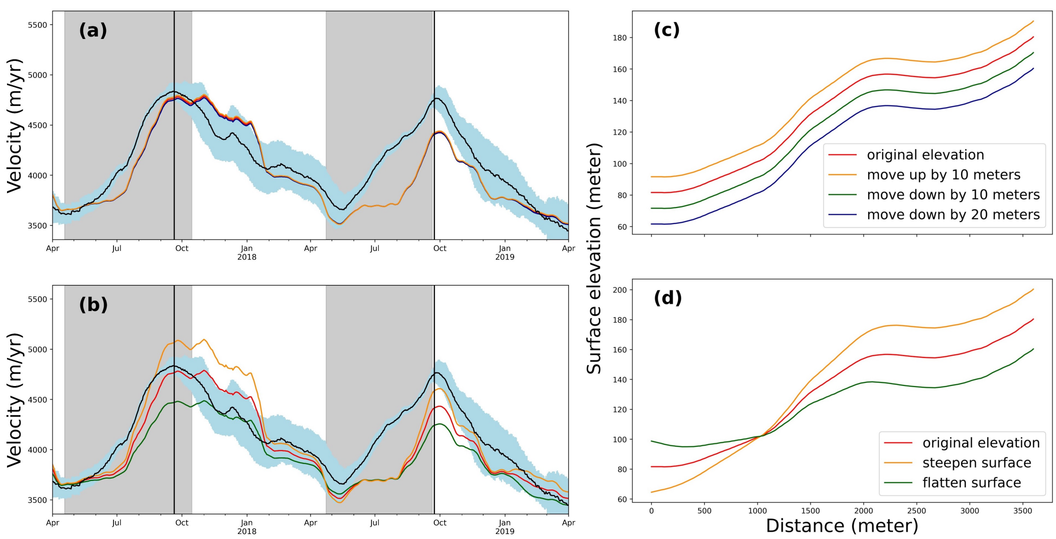

Figure 9. Experiment results using the artificially modified surface elevations. The results of (a) correspond to (c), and the results of (b) correspond to (d).

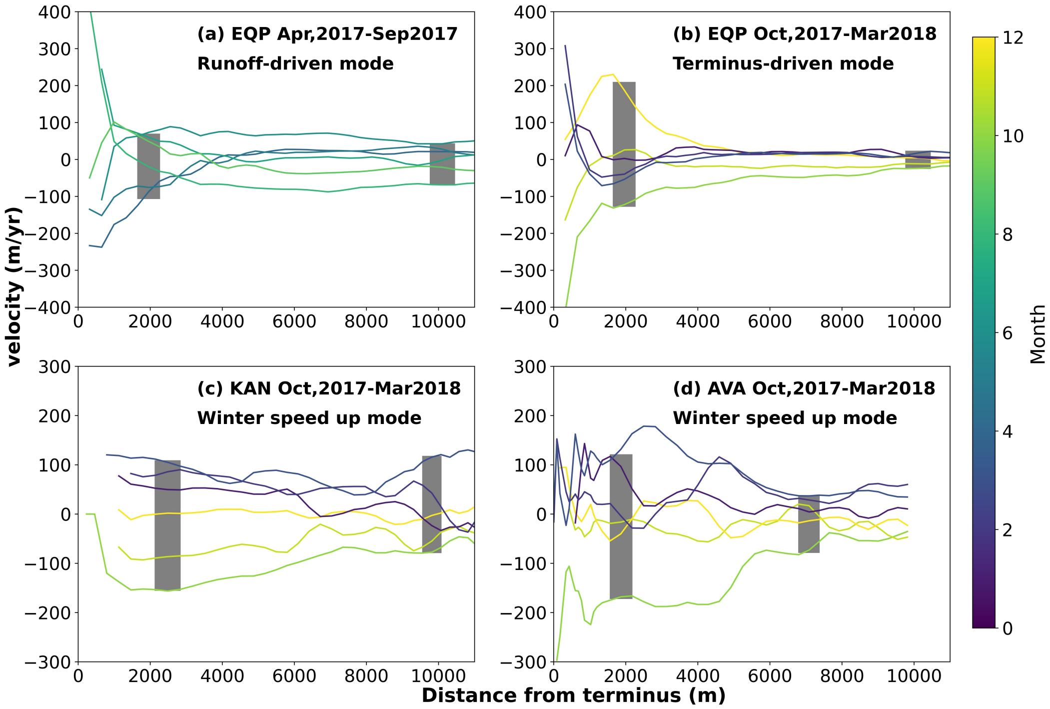

Figure 10. Velocity profiles over time for EQP, KAN, and AVA. The average velocity profile has been subtracted for a better display of changes over time. The original velocity profiles are shown in Figure S8. The shaded areas indicate regions where we obtain velocity variations in the frontal and upstream sections. (a) Velocity profiles of EQP during the melt season. (b) Velocity profiles of EQP after the melt season, during which velocity is primarily influenced by terminus changes. (c) Velocity profile of KAN during winter and early melt season. (d) Velocity profile of AVA during winter and early melt season.